

Velocity fluctuations in a steadily sheared model foamIan K. Ono,¹ Shubha Tewari,² Stephen A. Langer,³ and Andrea J. Liu¹¹*Department of Chemistry and Biochemistry, ULCA, Los Angeles, California 90095-1569, USA*²*Department of Physics, Mount Holyoke College, South Hadley, Massachusetts 01075-1440, USA*³*Information Technology Laboratory, NIST, Gaithersburg, Maryland 20899-8910, USA*

(Received 6 February 2002; revised manuscript received 27 March 2003; published 18 June 2003)

Numerical simulations are conducted to calculate velocity fluctuations in a simple two-dimensional model of foam under steady shear. The width of the velocity distribution increases sublinearly with the shear rate, indicating that velocity fluctuations are large compared to the average flow at low shear rates (stick-slip flow) and small compared to the average flow at large shear rates. Several quantities reveal a crossover in behavior at a characteristic strain rate $\dot{\gamma}_x$, given by the yield strain divided by the duration of a bubble rearrangement event. For strain rates above $\dot{\gamma}_x$, the velocity correlations decay exponentially in space and time, and the velocity distribution is a Gaussian. For strain rates below $\dot{\gamma}_x$, the velocity correlations decay as stretched exponentials in space and time, and the velocity distribution is broader than a Gaussian.

DOI: 10.1103/PhysRevE.67.061503

PACS number(s): 83.80.Iz, 83.80.Hj, 83.80.Fg, 64.70.Pf

I. INTRODUCTION

A foam or emulsion is a dispersion of easily deformable bubbles of a gas or droplets of a liquid [1–4]. When packed above the close-packing density, the bubbles or droplets deform away from the spherical shape and adjust their positions and shapes in order to minimize the total interfacial area. The resulting packing configuration lies in some local energy minimum. The typical energy barrier to rearrange bubble configurations is of the order of $\Sigma(\gamma_y R)^2$, where Σ is the interfacial tension, γ_y is the yield strain (of the order of a few percent for three-dimensional foams [5] or emulsions [6,7]), and R is the typical bubble size. The thermal energy is roughly 10^5 – 10^7 times smaller than the characteristic energy barrier height for typical bubble sizes (microns or larger). As a result, the bubbles cannot spontaneously rearrange and explore the phase space in search of a global energy minimum. When foam is sheared, however, enough energy is supplied to the system to overcome the energy barriers and bubbles can rearrange. As a result, foam yields and flows under a sufficiently high applied shear stress.

This paper is one of a series [8–12] that explore the question of how a simple two-dimensional model foam [8] yields under steady shear flow. The behavior depends on the packing fraction of bubbles, ϕ . Simulations on the quiescent system [13,8,9,14] show that there is a special packing fraction ϕ^* near random close packing, above which the pressure and shear modulus of the system are nonzero. Above $\phi^* \approx 0.84$ (in two dimensions), the system is therefore jammed [15]; it has a nonzero yield stress in a disordered state. In this paper, we will concentrate on the regime above ϕ^* . In this regime, experiments on three-dimensional foams [5,16], and emulsions [6], two-dimensional foams [17,18], and numerical simulations of the model [8–12] show that the nature of foam flow depends on the rate at which it is sheared. At very low shear strain rates, the flow is characterized by localized, intermittent rearrangement events that occur at a rate proportional to the strain rate. In these rearrangement events, the bubbles move from one stable, disordered packing configuration

(one local energy minimum) to another. Similar strain-induced rearrangement events have been seen in Lennard-Jones mixtures at low temperatures [19]. At high shear strain rates, on the other hand, the flow is smooth and laminar, with all the bubbles continually rearranging. The crossover between the two regimes occurs at the shear rate $\dot{\gamma}_x \approx \gamma_y / \tau_d$, where γ_y is the yield strain and τ_d is the duration of a rearrangement event.

In this paper, we focus on fluctuations of the velocities of individual bubbles around the average velocity profile. We study three main quantities: time correlations of velocity fluctuations, spatial correlations of velocity fluctuations, and the distribution of velocity fluctuations. We find a clear crossover in the behavior of these quantities at the characteristic strain rate $\dot{\gamma}_x$. At shear rates higher than $\dot{\gamma}_x$, where the flow is smooth, the velocity fluctuation distribution is Gaussian and the velocity correlations decay exponentially in space and time. Below $\dot{\gamma}_x$, where the flow is intermittent, the distribution is broader than the Gaussian and the velocity correlations decay more slowly than exponentially in both space and time. This striking change in dynamical behavior with decreasing strain rate $\dot{\gamma}$ is apparently unaccompanied by any diverging length scale and appears to be a signature of the approach to jamming.

In Sec. II, we review the model, the numerical methods used to solve it, and the quantities calculated. Sections III and IV contain our results. Section V is a discussion of the extent to which ideas from statistical mechanics can be applied to the collective behavior of this driven, athermal systems.

II. MODEL AND METHOD**A. Model**

Our simulations are carried out on a two-dimensional version of a model introduced by Durian [8,9]. The model and the numerical method we have used is discussed elsewhere [10], so our description here will be brief. The foam is de-

scribed entirely in terms of the bubble radii and the time-dependent positions of the bubble centers. The details of the microscopic interactions at the level of soap films and vertices are subsumed into two pairwise additive interactions between bubbles, which arise when the distance between bubble centers is less than the sum of their radii. The first, a repulsion that originates at the cost of energy to distort bubbles, is modeled by the compression of two springs in series with individual spring constants that scale with the Laplace pressures σ/R_i , where σ is the liquid-gas surface tension and R_i is the radius of bubble i . Bubbles that do not overlap are assumed not to interact. The second interaction is the viscous dissipation due to the flow of liquid in the films. It, too, is assumed to be pairwise additive and is modeled by a drag force proportional to the velocity difference between overlapping bubbles. We simplify this further by using the mean-field approximation, also employed by Durian [8–10], in which the drag force is proportional to the difference between the velocity of a bubble and the average flow at the position of the bubble. In a previous study, we found that the mean-field approximation makes no difference to the statistics of rearrangement events [10], despite the fact that the mean-field version of the model is not Galilean invariant. We note that the mean-field version is a better reflection of the physics of a two-dimensional monolayer foam experiment, where shear is applied indirectly to the monolayer by shearing the water subphase. Such experiments have been carried out by Dennin and co-workers [17,18].

We study a two-dimensional foam periodic in the x direction and trapped between parallel plates in the y direction. Bubbles that touch the top and bottom plates are fixed to them, and the top plate is moved at a constant velocity in the x direction. Thus, bubbles are divided into two categories—“boundary” bubbles, which have velocities that are determined by the motion of the plates, and “interior” bubbles, whose velocities must be determined from the equations of motion. We have checked our results by using periodic boundary conditions, with Lees-Edwards boundary conditions for steady-state shear, and have found that the different boundary conditions lead to only small quantitative differences. We use the SPARSKIT2 [20] library for sparse matrix solutions and the Runge-Kutta algorithm with a variable time step determined by the error tolerance to integrate the coupled differential equations of motion.

To introduce polydispersity, the bubble radii are drawn at random from a flat distribution of variable width; in all the results reported here, the bubble radii vary from 0.6 to 1.4 times the average bubble radius. The shape of the bubble size distribution appears to have no effect on viscoelasticity [9] or the statistics of rearrangement events [10] as long as it is sufficiently broad. Note that it is important to include polydispersity because a monodisperse system will crystallize under shear, especially in two dimensions.

In all our runs, the system is first equilibrated with all bubbles treated as interior bubbles, and with a repulsive interaction between the bubbles and the top and bottom plates so that the bubbles cannot penetrate the plates. The bubbles that touch the top and bottom plates are then converted to boundary bubbles.

B. Units

We will use dimensionless quantities throughout. Thus, r represents the distance in units of the average bubble diameter d and t represents the time in units of a characteristic time scale in the model, τ_d , set by the spring constant and the friction coefficient. This is the characteristic relaxation time arising from the competing mechanisms for elastic storage and viscous dissipation, and it measures the duration of a rearrangement event. Similarly, $\dot{\gamma}$ represents the shear rate multiplied by τ_d . Thus, $\dot{\gamma}$ is the Deborah number or, equivalently for this system, the capillary number. Energies are measured in units of Σd^2 , where Σ is the interfacial tension.

C. Quantities calculated

When the system is under steady shear with the velocity in the x direction and the velocity gradient in the y direction, the average velocity profile is linear: $\langle \mathbf{v}(y) \rangle = \dot{\gamma} y \hat{\mathbf{x}}$, where y ranges from zero at the bottom plate to L at the top plate. Note that we have imposed a linear profile by adopting the mean-field approximation, where the drag force is proportional to the deviation of the bubble velocity from the linear shear profile. However, in earlier work we showed that the average velocity profile is linear even if the mean-field approximation is not adopted and shear is imposed by the boundary [10]. Most experiments on sheared foam have also observed an average velocity profile that is linear [5,6,17,16,18,21], but one experiment has observed shear banding [22]. It is possible that shear banding was observed in the latter experiment due to the nonuniform stress in their radial Couette geometry, but further experiments should be done to resolve this question.

Our main focus is on the fluctuations around the average linear profile. To eliminate initial transients, we measure the average velocity profile. Once the measured profile is within 5% of the expected linear profile, we begin to collect data. We measure fluctuations of individual bubble velocities around the average profile. Thus, we define $\Delta \mathbf{v}(\mathbf{r}, t) \equiv \mathbf{v}_i(\mathbf{r}, t) - \dot{\gamma} y_i(\mathbf{r}, t) \hat{\mathbf{x}}$, where $\mathbf{v}_i(\mathbf{r}, t)$ and $y_i(\mathbf{r}, t)$ are the velocity and height, respectively, of bubble i centered at position \mathbf{r} at time t . We concentrate on three quantities: (1) the autocorrelation function $\langle \Delta \mathbf{v}(t) \cdot \Delta \mathbf{v}(0) \rangle$; (2) the equal-time spatial correlation function $\langle \Delta \mathbf{v}(\mathbf{r}) \cdot \Delta \mathbf{v}(\mathbf{0}) \rangle$; and (3) the distribution $P(\Delta v)$.

The Durian model contains two key features that allow it to display nontrivial velocity correlations. First, it is not an equilibrium system; it is in steady state. Second, the bubble packings are disordered.

For an equilibrium thermal system with a Hamiltonian, the velocity autocorrelation function is nontrivial, but the spatial correlation function always satisfies $\langle \Delta \mathbf{v}(\mathbf{r}) \cdot \Delta \mathbf{v}(\mathbf{0}) \rangle = \delta(\mathbf{r})$, where $\delta(\mathbf{r})$ is the Dirac-delta function. The velocity of bubble i is always completely uncorrelated with the velocity of bubble j , unless $i=j$, because of the separation between position and momentum degrees of freedom in the Hamiltonian. In addition, the velocity distribution is always Gaussian (the Maxwell-Boltzmann distribution).

It is important that we are studying disordered bubble packings. In a periodic packing, the energy increases when the system distorts affinely, and the energy drops when all the bubbles rearrange simultaneously. In a disordered foam, however, the deformation is nonaffine and some bubbles shift their relative positions to avoid distorting. This also allows nontrivial velocity distributions and correlations.

We study fairly small systems, typically 64, 225, or 625 bubbles. To obtain adequate statistics, averages (indicated by angular brackets) are taken over configurations as well as over time. For the velocity distributions $P(\Delta v)$, each distribution is collected over 1000–10 000 time steps, covering a total strain of at least 10, for at least nine different initial configurations. For the correlation functions at strain rates below $\dot{\gamma}_x$, we average over at least 10 000 time steps covering a total strain of 10 for ten different initial configurations. At or above $\dot{\gamma}_x$, however, we average over at least 5000 time steps covering a total strain of 10 for only five different initial configurations because very little variation with configuration is found. Error bars are based on variations among runs with different initial configurations as well as fluctuations within each run.

The magnitude of the correlation functions at $\mathbf{r}=\mathbf{0}$ or at $t=0$ is the mean-squared velocity fluctuation $\langle(\Delta v)^2\rangle$. This varies by several orders of magnitude over the range of shear rates studied. In plotting our results, it is convenient to scale the correlation functions by $\langle(\Delta v)^2\rangle$ so that we can show results for several different shear rates at once. Accordingly, we define the scaled correlation functions

$$F(\mathbf{r}) = \langle \Delta \mathbf{v}(\mathbf{r}) \cdot \Delta \mathbf{v}(\mathbf{0}) \rangle / \langle (\Delta v)^2 \rangle,$$

$$C(t) = \langle \Delta \mathbf{v}(t) \cdot \Delta \mathbf{v}(0) \rangle / \langle (\Delta v)^2 \rangle. \quad (1)$$

In addition to studying velocity correlation functions, we also examine several velocity fluctuation distributions. We have separated the x and y components to obtain $P(\Delta v_x)$ and $P(\Delta v_y)$ separately. We will show below that $P(\Delta v_x)$ and $P(\Delta v_y)$ are very similar. However, the calculation of Δv_x requires subtraction of the average shear profile, which introduces some error, so we focus on $P(\Delta v_y)$. We also compute two other distributions $P_{up}(\Delta v_y)$ and $P_{dn}(\Delta v_y)$. In Durian's model, the distortion of bubbles is measured globally by the total elastic energy stored in all the springs connecting overlapping bubbles. The distributions $P_{up}(\Delta v_y)$ and $P_{dn}(\Delta v_y)$ contain velocity fluctuations that occur when the elastic energy is increasing and decreasing, respectively. The rationale for separating the two distributions is based on a speculation on the nature of bubble motion under shear. Suppose we begin with a system in a local energy minimum. Under a small applied shear strain, the bubbles will distort. As the shear strain increases, the packing configuration eventually becomes unstable and bubbles rearrange their relative positions. Figure 1(a) shows a plot of the total elastic energy as a function of strain for a system driven at a constant shear rate of $\dot{\gamma}=10^{-5}$. Similar plots for stress vs strain are shown in Refs. [8,10]. Under steady shear, the elastic energy rises as bubbles distort (overlap) and then drops as bubbles rearrange. Figure 1(b) shows that the average slope of an energy

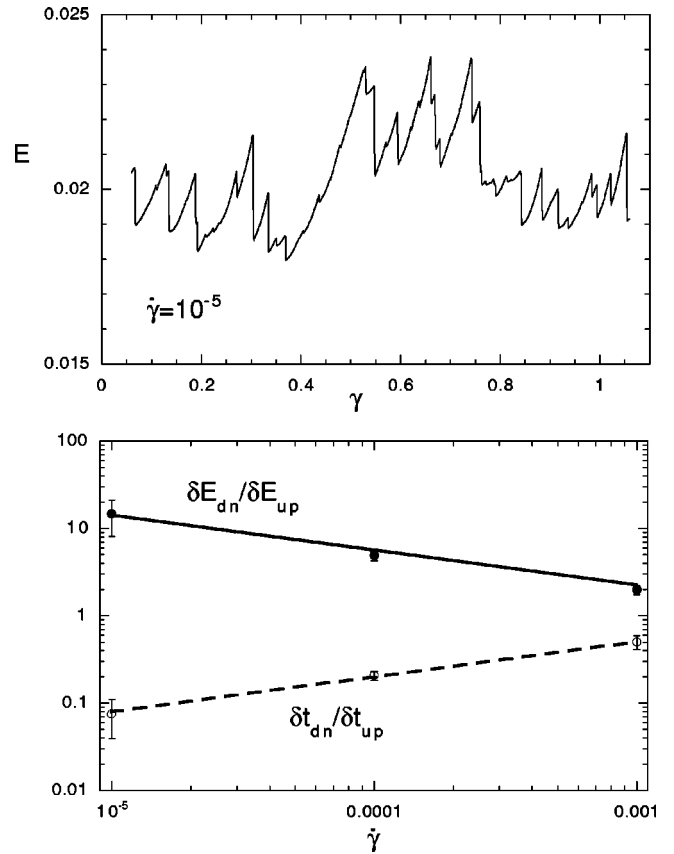


FIG. 1. (a) Total potential energy as a function of strain for a 225-bubble system at area fraction $\phi=0.9$ driven at a constant shear rate of $\dot{\gamma}=10^{-5}$. Note that the elastic energy increases gradually as bubbles increase the amount of overlap (deform), and decreases precipitously due to intermittent bubble rearrangement events. (b) Characteristics of energy drops relative to energy rises as a function of shear rate. Solid circles: the average time derivative of an energy drop relative to the average time derivative of an energy rise. The solid line is a fit to a power law with exponent -0.4 . Open circles: the average duration of an energy drop relative to the average duration of an energy rise. The dashed line is a fit to a power law with exponent 0.4 . This shows that a negligible fraction of time is spent on energy drops (bubble rearrangements) in the zero shear rate limit.

drop δE_{dn} decreases relative to the average slope of an energy rise δE_{up} as the shear rate $\dot{\gamma}$ increases. Conversely, the average duration of an energy drop δt_{dn} increases relative to the average duration of an energy rise δt_{up} as the shear rate increases. The straight lines are fits to the power laws $\delta E_{dn} / \delta E_{up} = 0.14 \dot{\gamma}^{-0.4}$ and $\delta t_{dn} / \delta t_{up} = 7.9 \dot{\gamma}^{0.4}$. Thus, in the limit of vanishing shear rate, energy drops (bubble rearrangements) occur infinitely rapidly relative to the energy rises (bubble distortions).

By sorting the velocity fluctuations into two distributions depending on whether the energy is rising or dropping, we can examine separately the bubble motion during distortion and rearrangement events. Note that the separation is not entirely clean because we compute only the *total* elastic energy of the system; because events can be localized and intermittent, the elastic energy may drop in one region of the

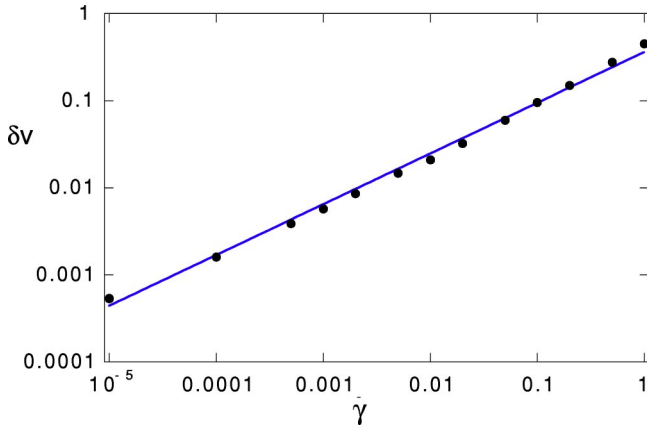


FIG. 2. Standard deviation of the y -velocity distribution as a function of shear rate. The width of the distribution narrows with decreasing shear rate. The line is a fit to a power law with exponent 0.6.

sample and rise in other regions. However, large rearrangement events involving large drops of energy should still be isolated in P_{dn} . Moreover, since a vanishing fraction of time is spent on energy drops in the zero shear rate limit, the total velocity fluctuation distribution approaches P_{up} in that limit.

III. RESULTS: VELOCITY CORRELATION FUNCTIONS

In defining the correlation functions $C(t)$ and $F(r)$ in Eq. (1), we have scaled the actual correlation functions by their zero-time or zero-separation values $\langle(\Delta v)^2\rangle$. This quantity has a strong shear rate dependence. In Fig. 2, we plot the standard deviation $\delta v \equiv \sqrt{\langle(\Delta v_y)^2\rangle}$ (similar results are obtained for velocity fluctuations in the x direction). The straight line is a fit to a power law with exponent 0.6; this provides an adequate fit, but note that there is a systematic upwards curvature in the data on this log-log plot, suggesting a more complex dependence on shear rate. Recent experiments on driven granular materials observe similar power-law scaling of velocity fluctuations [23–26]. This scaling is interesting because it implies that fluctuations diverge relative to the average flow in the limit of zero average flow. We will discuss the significance of this scaling in detail in Sec. V C.

In an equilibrium system $\delta v^2 \equiv T/m$, where the Boltzmann constant is unity, T is the temperature, and m is the particle mass. It is tempting to associate an effective temperature with δv based on this relation. However, there is no inertia in our system so the mass m is undefined. In previous papers, we have calculated an effective temperature T_{eff} based on linear response relations [11,12]. If we compare δv to T_{eff} , we find that they have very different shear rate dependences. Figure 2 shows that δv decreases with decreasing $\dot{\gamma}$ and appears to vanish as $\dot{\gamma} \rightarrow 0$. In contrast, we find that T_{eff} appears to level off to a constant value at low $\dot{\gamma}$ [11,12]. If we associate δv with a temperature, this would imply that the effective mass m of the bubbles must diverge in the limit $\dot{\gamma} \rightarrow 0$. This is probably not a sensible interpretation of the results. It is more reasonable to conclude that since there is

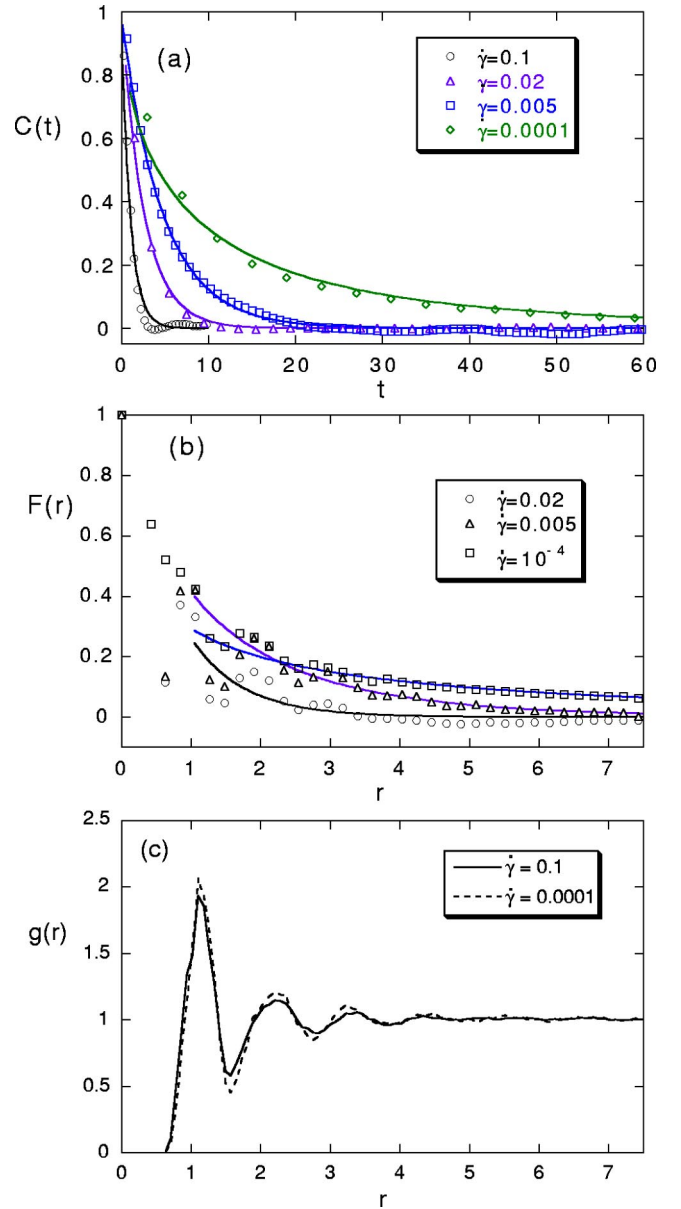


FIG. 3. Correlation functions. (a) The velocity autocorrelation function $C(t)$ [Eq. (1)]; (b) the velocity correlation function $F(r)$, Eq. (1); (c) the radial distribution function $g(r)$. In all three plots, the correlation functions are shown for several different shear rates, as marked. The curves in plots (a) and (b) represent fits of the tails to Eqs. (2) and (4), respectively.

no kinetic energy in our system, we cannot extract an effective temperature from velocity fluctuations.

A. Shape of correlation functions

Several correlation functions are shown in Fig. 3 for 225-bubble systems at $\phi=0.9$ at several different strain rates. In Figs. 3(a) and 3(b), we plot the scaled velocity autocorrelation function $C(t)$ and the scaled velocity correlation function $F(r)$, defined in Eq. (1). In Fig. 3(c), we plot the pair correlation function $g(r)$.

In an equilibrium liquid, $C(t)$ is nonmonotonic and dips below zero [27]. The dip is attributable to short-ranged re-

pulsive interactions that push particles away from each other. The function $F(r)$, on the other hand, is identically zero in an equilibrium system since the velocities of different particles are uncorrelated. Finally, the pair correlation function $g(r)$ in an equilibrium system is very similar to the one we calculate for the sheared system.

In examining Fig. 3, first note that $g(r)$ is nearly independent of $\dot{\gamma}$, while $C(t)$ and $F(r)$ are much more sensitive to $\dot{\gamma}$. Thus, there is no noticeable change in structure, but there is a significant change in the dynamics with decreasing shear rate.

The velocity autocorrelation function $C(t)$ does not always decay monotonically with time at all shear rates, as shown in Fig. 3(a). We find that $C(t)$ dips below zero at high shear rates, $\dot{\gamma} \geq 0.05$. At high shear rates, the behavior of the foam is liquidlike, with all the bubbles rearranging all the time. The repulsive spring interactions between bubbles should lead to dips in the velocity fluctuation autocorrelation function in this regime since the packing fraction is high ($\phi = 0.9$ in Fig. 3). In other words, a bubble will reverse direction relative to the average shear when it approaches a neighboring bubble too closely. This picture is supported by the behavior of spatial correlations in the velocity. The scaled correlation function $F(r)$ is nonmonotonic and can even be negative for $\dot{\gamma} \geq 0.05$. At $\dot{\gamma} = 0.1$, the first dip in $F(r)$ occurs in the first neighbor peak of $g(r)$. Thus, neighboring bubbles tend to move in opposite directions, as expected due to the repulsive interactions.

It is more surprising that there is *not* a dip in $C(t)$ at lower shear rates [see Fig. 3(a)], since the packing fraction is still high and the repulsive interactions between bubbles are even stronger relative to viscous interactions at low shear strain rates. Some insight can be gained by studying the spatial correlation function $F(r)$, shown in Fig. 3(b). At lower shear rates, $F(r)$ is positive at all r . Thus, neighboring bubbles tend to move in the same direction at lower shear rates. This is in marked contrast to the velocity autocorrelation function for an equilibrium liquid, which is always nonmonotonic because the kinetic energy of particles leads to collisions. This correlation in the motion of nearby bubbles implies that a bubble does not have to reverse direction when it travels a distance comparable to the interbubble spacing. Thus, it is possible for $C(t)$ to decay monotonically.

The curves shown in Fig. 3(a) represent fits of $C(t)$ to the function,

$$C(t) = \exp[-(t/\tau_1)^{\beta_t}], \quad (2)$$

where τ_1 and β_t are fitting parameters. This function evidently provides a reasonable fit as long as the correlation function is always positive, and it gives a fairly good fit to the envelope when the correlation function dips below zero. The fitting parameters are shown in Fig. 4(a). The exponent β_t (circles) starts at unity at high shear rates, and crosses over to 0.6 at low shear rates. Meanwhile, the parameter τ_1 (triangles) increases by one order of magnitude with decreasing shear rate, and levels off at around $\dot{\gamma} = 0.001$.

An alternate fitting function provides fits that are indistin-

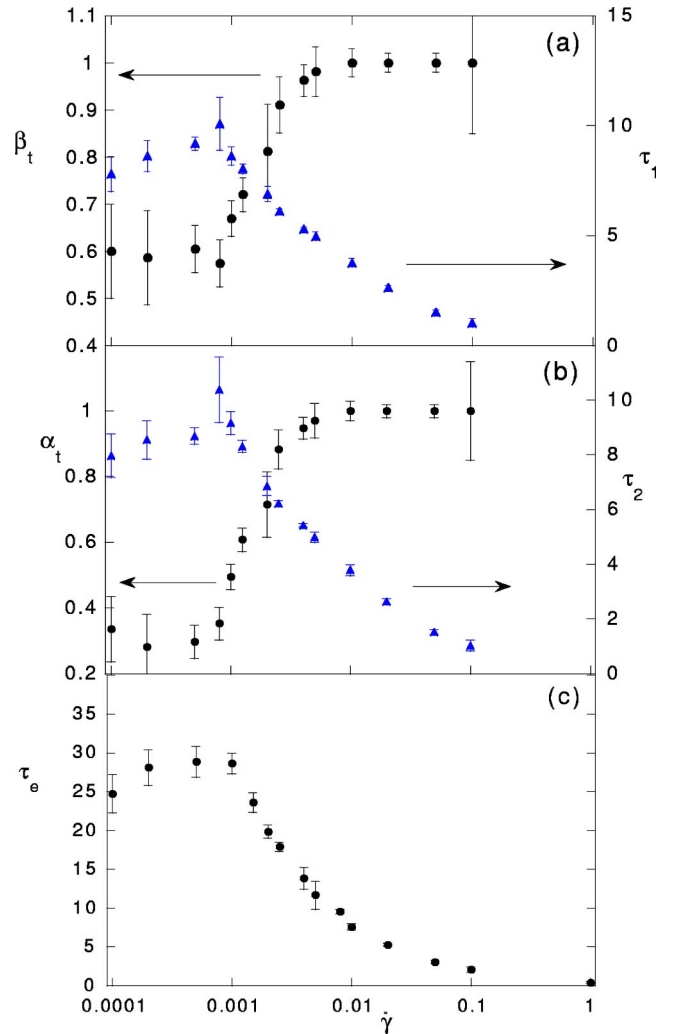


FIG. 4. Fitting parameters for the velocity autocorrelation function $C(t)$ as a function of shear rate. (a) Fitting parameters to Eq. (2), where β_t (circles) is the stretching exponent and τ_1 (triangles) is the relaxation time. (b) Fitting parameters to Eq. (3), where α_t (circles) is the coefficient of the exponential term and τ_2 (triangles) is the relaxation time. (c) The time τ_e over which $C(t)$ decays to $1/e^2$. This increases with decreasing shear rate, but saturates at $\dot{\gamma} \approx 10^{-3}$.

guishable from those provided by Eq. 2 in Fig. 3(a). This form is a linear combination of an exponential and a stretched exponential:

$$C(t) = \alpha_t \exp[-t/\tau_2] + (1 - \alpha_t) \exp[-\sqrt{t/\tau_2}], \quad (3)$$

where α_t and τ_2 are fitting parameters. The results for α_t are shown as circles in Fig. 4(b). Evidently, $C(t)$ is a pure exponential at shear rates above $\dot{\gamma} \approx 0.01$, and crosses over to nonexponential behavior at low shear rates. The behavior of τ_2 (triangles) from this fit is very similar to the behavior for the fit to Eq. (2). Note that the fitting parameters τ_1 and τ_2 are not a very good measure of the relaxation time since the form of the fit changes with shear rate. We therefore define the relaxation time τ_e as the time in which $C(t)$ decays to $1/e^2$. This definition is arbitrary; we have avoided the more

standard choice of the decay to $1/e$ because it is important to include the difference between exponential and stretched-exponential decay. The time scale τ_e is plotted in Fig. 4(c). The behavior of τ_e is qualitatively similar to that of τ_1 and τ_2 , but τ_e increases by a larger factor over the range of shear rates studied.

From these fits in Fig. 4, we conclude that the autocorrelation function has several distinct regimes: (1) At high shear rates ($\dot{\gamma} \geq 0.05$), $C(t)$ dips below zero; this is similar to the behavior in an equilibrium liquid. (2) At intermediate shear rates ($0.01 \leq \dot{\gamma} < 0.1$), $C(t)$ decays exponentially with a decay time that increases with decreasing shear rate. (3) At lower shear rates ($0.001 < \dot{\gamma} < 0.01$), $C(t)$ crosses over to a broader-than-exponential decay and the decay time continues to increase. (4) At low shear rates ($\dot{\gamma} < 0.001$), the scaled correlation function $C(t)$ appears to become independent of shear rate. (Note that the velocity autocorrelation function itself, $\langle (\Delta v)^2 \rangle C(t)$, still depends on shear rate because the amplitude $\langle (\Delta v)^2 \rangle$ depends on $\dot{\gamma}$, as shown in Fig. 2.) We suspect that the reason why $C(t)$ appears to saturate at low $\dot{\gamma}$ is that it is dominated (particularly at short times) by the dynamics during rearrangement events. As $\dot{\gamma}$ decreases, rearrangement events occur less frequently. Since bubbles are hardly move when they are not rearranged, the contribution to the velocity autocorrelation is very small, except during rearrangement events. Therefore, the amplitude of the velocity autocorrelation function decreases. Since the main contribution to the autocorrelation function still comes from rearrangement events, the shape of $C(t)$ remains the same at short times. At longer time scales, however, there should be a tail. We know that other autocorrelation functions, such as the stress autocorrelation function, decay more and more slowly as $\dot{\gamma}$ decreases, with a time scale $\tau_\alpha \approx 1/\dot{\gamma}$. This time scale also sets the magnitude of the viscosity. The velocity autocorrelation function should also reflect this slow relaxation time. Even in simulations of equilibrium liquids [27], this time scale is difficult to resolve because short-time features dominate the velocity autocorrelation function. We surmise that we do not observe the tail because the amplitude is similarly small in the sheared foam.

Similar behavior is observed in the spatial correlation function $F(r)$. The curves shown in Fig. 3(b) are fits of $F(r)$ to the function

$$F(r) = \exp[-(r/\xi_1)^{\beta_r}], \quad (4)$$

where ξ_1 and β_r are fitting parameters shown in Fig. 5(a). At high shear rates, the exponent β_r is unity, as shown by the circles in Fig. 5(a). Between $\dot{\gamma} \approx 0.02$ and $\dot{\gamma} \approx 0.001$, β_r drops to roughly 0.5. Meanwhile, the correlation length ξ_1 (triangles) increases slightly, but is essentially fixed around the bubble diameter at all shear rates.

We have also used an alternate fitting form for $F(r)$:

$$F(r) = \alpha_r \exp[-r/\xi_2] + (1 - \alpha_r) \exp[-\sqrt{r/\xi_2}], \quad (5)$$

where α_r and ξ_2 are fitting parameters. The quality of the fits is indistinguishable from those for Eq. (4). The resulting val-

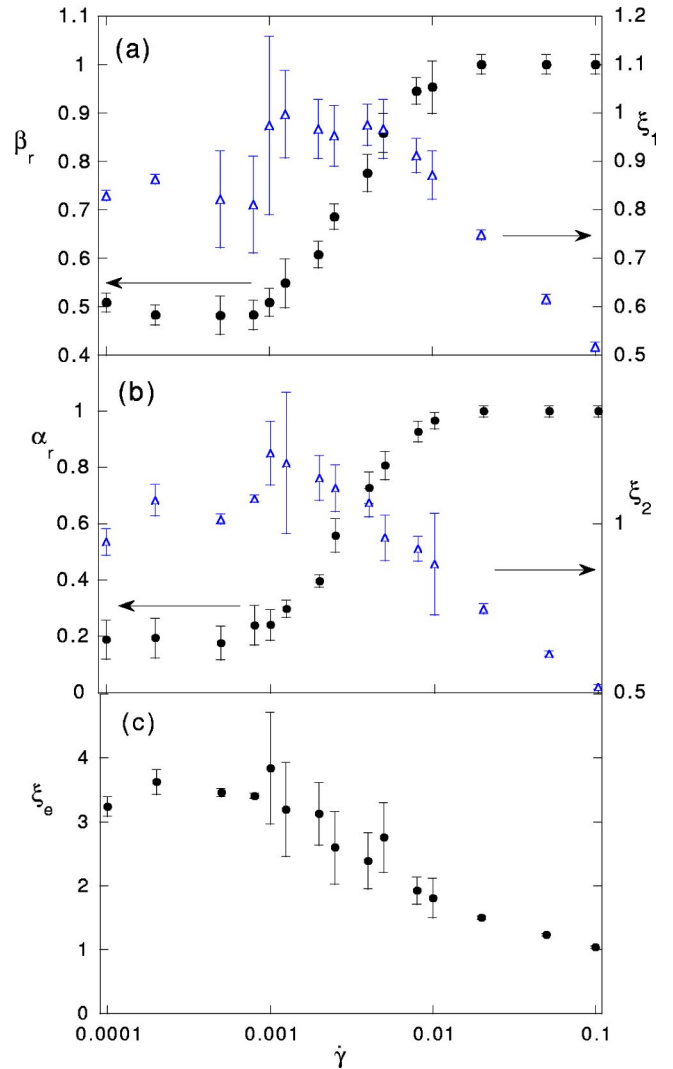


FIG. 5. Fitting parameters for the velocity correlation function $F(r)$ as a function of shear rate. (a) Fitting parameters to Eq. (4), where β_r (circles) is the stretching exponent and ξ_1 (triangles) is the correlation length. (b) Fitting parameters to Eq. (5), where α_r (circles) is the coefficient of the exponential term and ξ_2 (triangles) is the correlation length. (c) The distance ξ_e over which $F(r)$ decays to $1/e^2$.

ues of α_r and ξ_2 are shown as circles and triangles, respectively, in Fig. 5(b). The agreement between the results from the two fits, Eqs. (4) and (5), confirms that the spatial correlation function decays as an exponential at high shear rates, and as a stretched exponential at low shear rates, but that the correlation length remains short at all shear rates. We have also plotted ξ_e , the distance at which $F(r)$ decays to $1/e^2$, in Fig. 5(c). Note that ξ_e increases by only about a factor of 3 over four decades of shear rate, and is comparable to the average bubble diameter.

Why do we observe exponential decay of $C(t)$ and $F(r)$ at high shear rates and stretched exponential decay of $C(t)$ and $F(r)$ at low shear rates? In viewing movies of our simulations, we have observed that the rearrangement events are discrete and localized at low shear rates, but are continuous at high shear rates. The size of rearrangement events that we

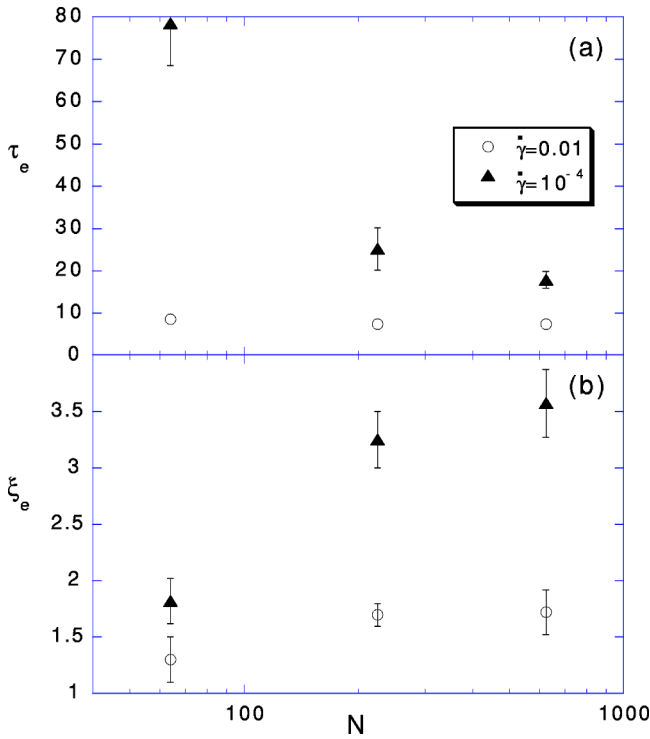


FIG. 6. System-size dependence. (a) The relaxation time τ_e , over which the velocity autocorrelation function $C(t)$ decays to $1/e^2$, at two different shear rates. At $\dot{\gamma}=10^{-4}$ (triangles), τ_e is independent of N . At $\dot{\gamma}=0.01$ (circles), τ_e decreases with increasing system size. (b) The correlation length ξ_e , over which $F(r)$ decays to $1/e^2$, at two different shear rates. At $\dot{\gamma}=10^{-4}$ (triangles), ξ_e increases with increasing N , but at $\dot{\gamma}=0.01$ (circles), ξ_e is independent of N .

observe is consistent with ξ_e , namely, of the order of a bubble diameter [10]. Similar results are seen in experiments on three-dimensional foams [5] and two-dimensional foams [17]. At low shear rates, when the flow is intermittent, there are, therefore, pronounced kinetic heterogeneities in the system. We believe that this gives rise to the stretched-exponential decay of $C(t)$ and $F(r)$, in much the same way as kinetic heterogeneities give rise to stretched-exponential decays of correlations in glassforming liquids.

1. System-size dependence

We have calculated the velocity correlations for three different system sizes: $N=64$, $N=225$, and $N=625$ bubbles, all at an area fraction $\phi=0.9$. The quantities τ_e and ξ_e are plotted as a function of N in Figs. 6(a) and 6(b) for two different shear rates $\dot{\gamma}=0.01$ and $\dot{\gamma}=10^{-4}$. We find that τ_e and ξ_e are independent of the system size at the higher shear rate $\dot{\gamma}=0.01$. At $\dot{\gamma}=10^{-4}$, however, τ_e decreases and ξ_e increases with the system size. For $N=64$, there is a pronounced difference in the correlation functions, but both τ_e and ξ_e appear to approach saturation for the two largest system sizes; their values for $N=225$ and $N=625$ overlap within the error bars.

Why do system-size effects appear at low shear rates, but not at high shear rates? At high shear rates, the correlations

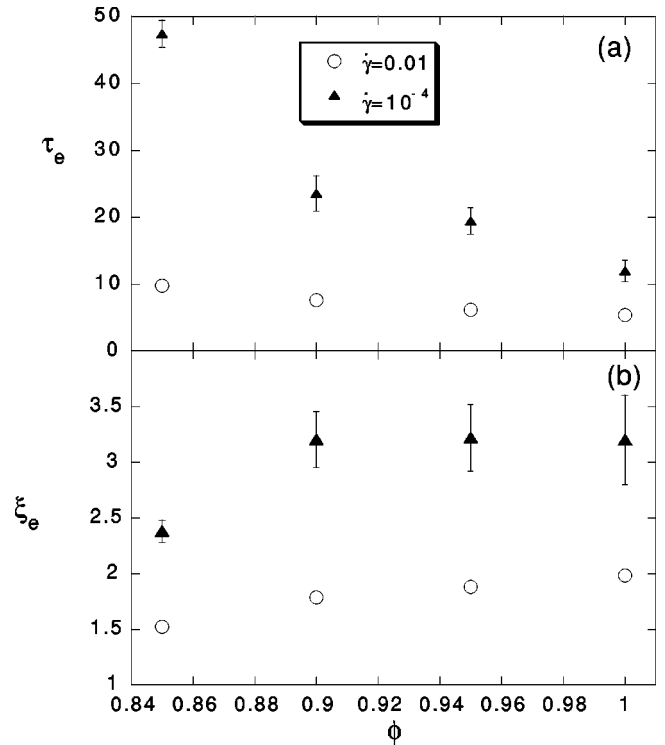


FIG. 7. Area fraction dependence. (a) The relaxation time τ_e as a function of ϕ at two different shear rates. At $\dot{\gamma}=10^{-4}$ (triangles), τ_e increases as ϕ decreases towards close packing. At $\dot{\gamma}=0.01$ (circles), τ_e is independent of ϕ . (b) The correlation length ξ_e is independent of ϕ at both $\dot{\gamma}=10^{-4}$ (triangles) and $\dot{\gamma}=0.01$ (circles). For $\dot{\gamma}=10^{-4}$, error bars are omitted because they are smaller than the symbols.

are short ranged and decay exponentially. On the scale of the system-size, there are no long-ranged correlations and therefore there are no system-size effects. At low shear rates, however, the correlations decay as a stretched exponential due to kinetic heterogeneities. At $\dot{\gamma}=10^{-4}$, we note that $F(r)$ has not decayed to zero on the scale of the system size in Fig. 3(b). In order to obtain a good average over the kinetic heterogeneities, one must study the system on length scales large as compared to the size of the heterogeneities (ξ_e). Therefore, there are slight differences between the 225-particle and 625-particle systems.

2. Area fraction dependence

Earlier studies [13,8–10,14], have suggested that there is a special point near random close packing ($\phi^*\approx 0.84$) and zero shear rate that has some properties reminiscent of a critical point (and others that are definitely unusual for a critical point [14]). At close packing, the pressure and shear modulus vanish as power laws [13,8,14], the stress relaxation time becomes very large [8], and the distribution of avalanche sizes appears to approach a pure power law [10]. Here, we examine the dependence of the correlation functions on area fraction. The correlation time and distance, τ_e and ξ_e , are shown in Figs. 7(a) and 7(b) for two different shear rates $\dot{\gamma}=0.01$ and $\dot{\gamma}=10^{-4}$. Evidently, the correlation

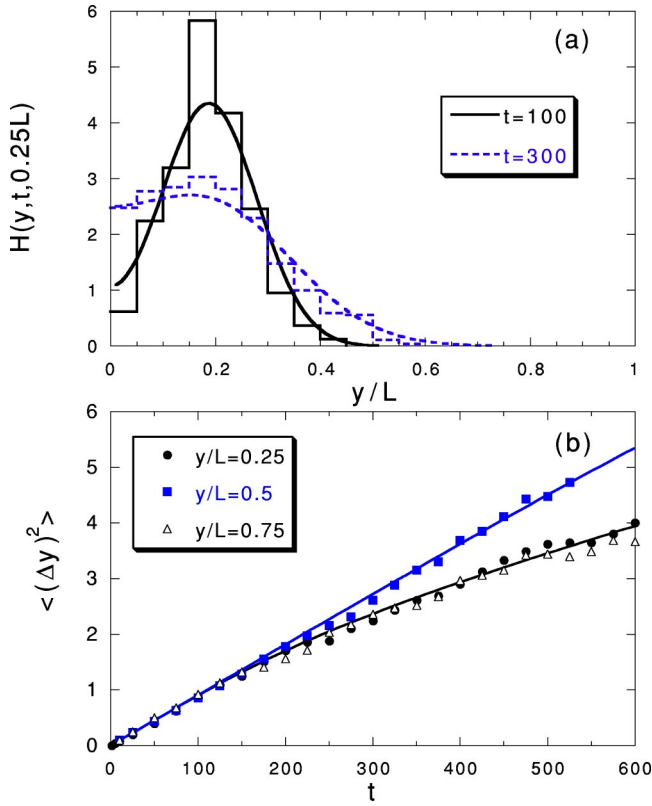


FIG. 8. (a) Distribution $H(y, t, y_i)$ of y coordinates of bubble positions at times $t=100$ (solid) and $t=300$ (dotted), given an initial position of $y_i=0.25L$. The curves are fits to the one-dimensional diffusion equation with the same diffusion coefficient at both times. (b) Mean-squared displacements in the y direction for initial y positions of $y_i=0.25L$ (circles), $y_i=0.5L$ (squares), and $y_i=0.75L$ (triangles). The curves are fit to the one-dimensional diffusion equation with the same diffusion coefficient as in (a) for all times and all y_i .

time τ_e increases in the double limit $\dot{\gamma} \rightarrow 0$ and $\phi \rightarrow \phi^*$, consistent with previous conclusions [8]. However, the correlation length ξ_e has no noticeable dependence on ϕ . Thus, ξ_e does not diverge as $\phi \rightarrow \phi^*$.

B. Transverse diffusion coefficient

As a check on our results for the velocity autocorrelation function, we have calculated the self-diffusion coefficient in the transverse (y) direction (i.e., *perpendicular* to the shear direction) in two different ways. First, we obtain it by integrating the velocity autocorrelation function over time. Second, we calculate the distribution of particle displacements in the y direction, $H(y, t, y_i)$, and fit the results to the one-dimensional diffusion equation with reflecting boundaries. Here, $H(y, t, y_i)$ is the probability of finding the particle at a time t after the particle was at y_i .

A typical result for the y -displacement distributions $H(y, t, y_i=0.25L)$, where L is the spacing between boundaries in the y direction, at two different time intervals at a shear rate of $\dot{\gamma}=0.05$ is shown in Fig. 8(a). The curves through the data are fits to the solution of the one-

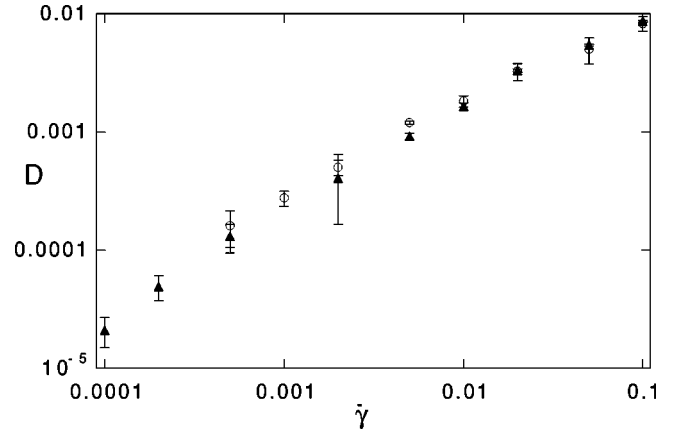


FIG. 9. Diffusion coefficient obtained from displacement distributions (open circles) and by integrating the velocity autocorrelation function over time (solid triangles) as a function of shear rate. The two results are the same, as expected. Note that the diffusion coefficient cannot be described as a pure power law in shear rate.

dimensional diffusion equation with reflecting boundaries. Both fits yield the same diffusion coefficient. We have also plotted the mean-squared displacement $\langle (y(t) - y_i)^2 \rangle$ as a function of time in Fig. 8(b) for three starting values for y_i , namely, $0.25L$, $0.5L$, and $0.75L$. By symmetry, the results for $y_i=0.25L$ and $y_i=0.75L$ must be the same, on an average, so this serves as a check on our statistics. The curves are fits to the data to the one-dimensional diffusion equation with a single fit parameter, namely, the diffusion coefficient D_y for all times and all y_i . The agreement between the simulation data and the curves shows that bubble motion in the transverse direction is diffusive.

We have also calculated the diffusion coefficient by integrating the velocity autocorrelation function according to the equation

$$D = \int_0^{\infty} \langle v_y(t) v_y(0) \rangle dt. \quad (6)$$

In Fig. 9, we plot the diffusion coefficient obtained by integrating the velocity autocorrelation function over time (solid triangles) as well as the diffusion coefficient obtained by fitting displacement distributions (open circles) for several different shear rates. The two results are in excellent agreement, as they ought to be.

Figure 9 shows that the diffusion coefficient decreases with decreasing $\dot{\gamma}$. This is similar to the behavior of the diffusion coefficient for a particle in an equilibrium liquid, which decreases with decreasing temperature. However, the velocity autocorrelation function, whose integral over time yields D , appears to be very different in the two cases. In liquids, D decreases precipitously with decreasing temperature because the positive and negative portions of $C(t)$ come closer to canceling each other, while the zero-time value of the correlation function $\langle \Delta v^2 \rangle$ decreases linearly with T as $2kT/m$. In the sheared foam, in contrast, the diffusion coefficient decreases with decreasing shear rate because the zero-time value of the correlation function $\langle \Delta v^2 \rangle$ decreases, while

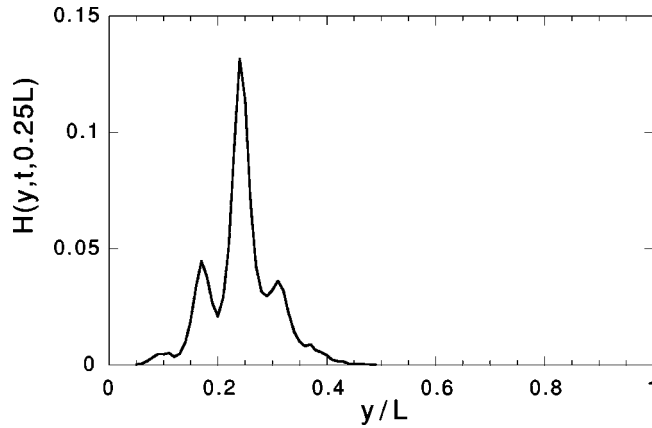


FIG. 10. Distribution of y coordinates of bubble positions at time $t=25$, given an initial position of $y_i=0.25L$, at high shear rate ($\dot{\gamma}=1$). The two peaks flanking the central peak show that the bubbles tend to get trapped in the y direction and do not simply diffuse; this is an evidence that the bubbles are organized into strings at high shear rate.

$C(t)$ is always positive (see Fig. 3). As discussed earlier, in dense liquids, $C(t)$ typically crosses over to a negative value on the collision time scale because the particles have kinetic energy.

At high shear rates, around $\dot{\gamma} \approx 1$, the displacement distribution does not appear to be diffusive (it cannot be fit by the solution to the one-dimensional diffusion equation with reflecting boundaries). A typical result for the displacement distribution in this regime is shown in Fig. 10. This figure is based on 20 000 different trajectories. Each trajectory begins at $y_0=0.25L$ and ends at some height y after a time interval of 25. Figure 10 is a histogram of the final y values. When we view movies of the simulations in this regime, we observe that the bubbles organize into strings that move in the \hat{x} direction. Similar strings have been observed in simulations of colloids under shear and are believed to be a system-size effect [28]. In our case, we find that the observed behavior depends on the boundary conditions; if we use periodic boundaries in the y direction instead of fixed boundaries, we find that strings do not form at $\dot{\gamma}=1$ and that the displacement distribution remains diffusive. Thus, the strings we observe appear to be finite system-size artifacts.

IV. RESULTS: VELOCITY DISTRIBUTION

In an equilibrium Hamiltonian system, the velocity distribution of particles is Gaussian with a width that depends on the temperature and the particle mass. In our driven dissipative system, there is no particle mass because we neglect inertia, and there are no thermal fluctuations. However, there are fluctuations that arise when the sheared bubbles jostle each other. The resulting distribution for the y component of the velocity (transverse to the shear) is shown in Fig. 11 for a 625-bubble system at $\phi=0.9$. The distributions $P_{up}(\Delta v_y)$ and $P_{dn}(\Delta v_y)$ (i.e., the distributions of y velocities incurred when the total elastic energy is increasing and decreasing, respectively; see Sec. II) appear qualitatively similar to the

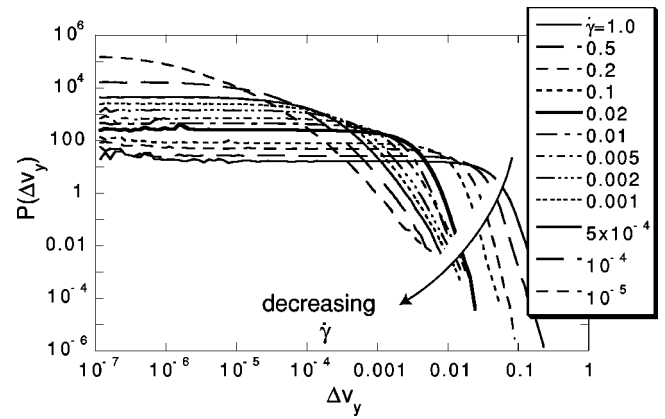


FIG. 11. Distribution of the y component of bubble velocities as a function of shear rate. The units for velocity in this plot correspond to L/τ_d . Note that at high shear rates ($\dot{\gamma} \geq 0.02$), the distribution narrows with decreasing $\dot{\gamma}$, but does not change shape. For $\dot{\gamma} < 0.02$, the distribution develops a tail at high velocities.

total distribution. In all cases, we calculate the distribution of the absolute value of the velocity because the distributions are symmetric in Δv_y . All three distributions show a qualitatively similar behavior; as $\dot{\gamma}$ decreases, the distributions become narrow. Above the crossover shear rate $\dot{\gamma}_c \approx 0.02$, the functional form of the distribution does not appear to depend on shear rate, but the width of the distribution decreases with decreasing $\dot{\gamma}$. Below $\dot{\gamma}_c$, the width of the distribution continues to decrease with decreasing $\dot{\gamma}$, but the distribution develops a progressively larger tail at high velocities. The dependence of the width of the distribution, δv , on shear rate was shown earlier in Fig. 2.

A. System-size dependence

Our results for $P_{up}(\Delta v_y)$ are independent of system size for the two sizes we have studied, namely, $N=225$ bubbles and $N=625$ bubbles, at an area fraction of $\phi=0.9$. This is illustrated in Fig. 12, which shows the distribution $P_{up}(\Delta v_y)$ for $N=225$ (symbols) and $N=625$ (lines) at three different shear rates, ranging from high to low. The slight difference at $\dot{\gamma}=10^{-5}$ is probably due to the fact that we have better statistics for the larger system.

B. Area fraction dependence

We have studied four different area fractions above the close-packing value of $\phi_c \approx 0.84$, namely, $\phi = 0.85, 0.90, 0.95, 1.0$. In these runs, the dimensions of the system were held fixed and the number of bubbles varied to change the packing fraction; at $\phi=1.0$, the system contains $N=250$ bubbles. The distribution $P_{up}(\Delta v_y)$ at a low shear rate $\dot{\gamma}=10^{-5}$ is shown for these different values of ϕ in Fig. 13(a). Interestingly, we find that for the three highest area fractions, the shape of the distribution is roughly the same, but for $\phi=0.85$, the area fraction closest to ϕ_c , the distribution has a noticeably different shape and is significantly narrower. This implies that the distribution is sensitive to the

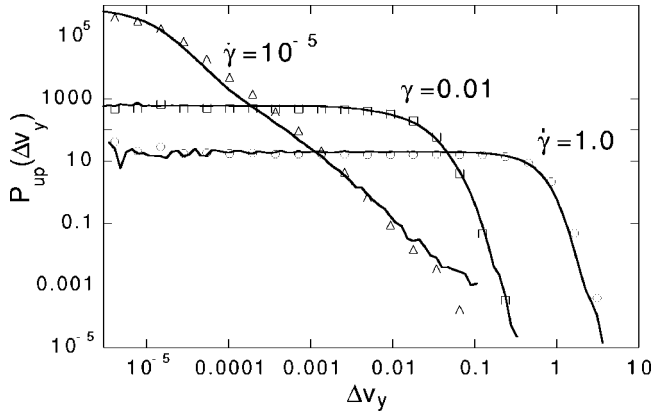


FIG. 12. The distribution $P_{up}(\Delta v_y)$, namely, the distribution of y velocities when the total energy increases as a function of system size. The area fraction is fixed at $\phi=0.9$. The symbols correspond to $N=225$ and the curves to $N=625$. At each shear rate, there is no significant difference between the results for the two different system sizes. Error bars are not shown if they are smaller than the symbol.

area fraction for ϕ close to ϕ_c , but is relatively insensitive to ϕ at values far above ϕ_c . It is not surprising that the distribution is narrower near ϕ_c ; the velocity fluctuations are driven by the repulsive interactions between bubbles, which

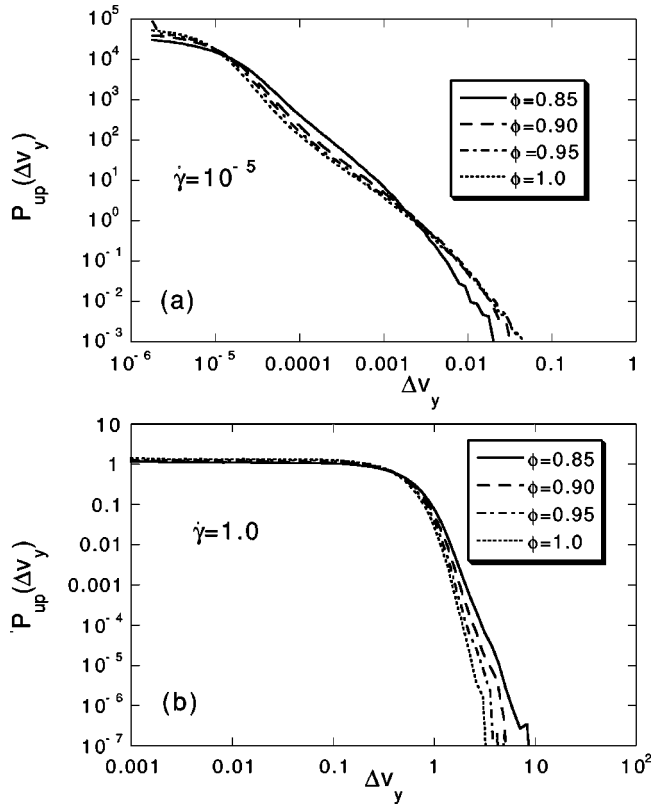


FIG. 13. Velocity distribution $P_{up}(\Delta v_y)$ as a function of area fraction ϕ . (a) At a low shear rate $\dot{\gamma}=10^{-5}$, the distribution is independent of ϕ for $\phi \geq 0.90$, but is slightly narrower near close packing at $\phi=0.85$. (b) At a high shear rate of $\dot{\gamma}=1.0$, the distribution widens slightly with decreasing ϕ .

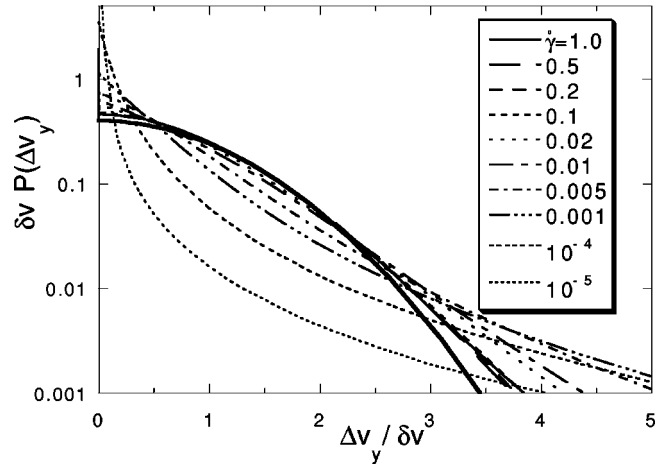


FIG. 14. Distribution of y velocities, $P(\Delta v_y)$, at different shear rates on a semilog plot. Here, the velocity Δv_y is scaled by δv , the standard deviation of the distribution. A Gaussian distribution is a half-parabola and is shown in gray. At high shear rates ($\dot{\gamma} \geq 0.01$), the distribution is approximately Gaussian. At lower shear rates, however, the velocity distribution develops a much broader tail.

get weaker as ϕ decreases because the bubbles are less tightly packed.

At high shear rates, we find that the width of the distribution increases slightly but systematically with decreasing area fraction, as shown in Fig. 13(b) for the distribution $P_{up}(\Delta v_y)$ at $\dot{\gamma}=1.0$. This is the opposite of the trend observed at low shear rates. At these high shear rates, viscous dissipation is much more important than the repulsive interactions between particles. As we saw from the displacement distribution in Fig. 10, particles tend to organize into strings along the shear direction that are held in place by the repulsive interactions; at high shear rates, repulsions therefore tend to suppress velocity fluctuations in the y direction. We surmise that due to this reason the distribution grows broader as the area fraction (and, correspondingly, the strength of repulsive interactions) decreases towards ϕ_c .

C. Shear rate dependence

The shape of the distribution changes markedly with shear rate. In Fig. 14, we have replotted $P(\Delta v_y)$ as a function of Δv_y on a semilog plot. Here, we have scaled Δv_y by the standard deviation of the distribution, δv , shown earlier in Fig. 2. At high shear rates, the distribution does look approximately Gaussian (a Gaussian distribution is plotted for comparison in heavy black; it is a half parabola on a semilog plot). This is not surprising, given our results for the velocity correlations in Sec. III; the velocity correlations decay very rapidly with separation at high shear rates so that different bubbles are essentially uncorrelated with each other. Therefore, the distribution is Gaussian, as it is in an equilibrium liquid. At lower shear rates, where velocities of different bubbles are correlated, the distribution clearly develops a non-Gaussian tail. Our results suggest the following picture: as the shear rate decreases, the scale of velocity fluctuations also decreases. However, once the flow becomes intermittent

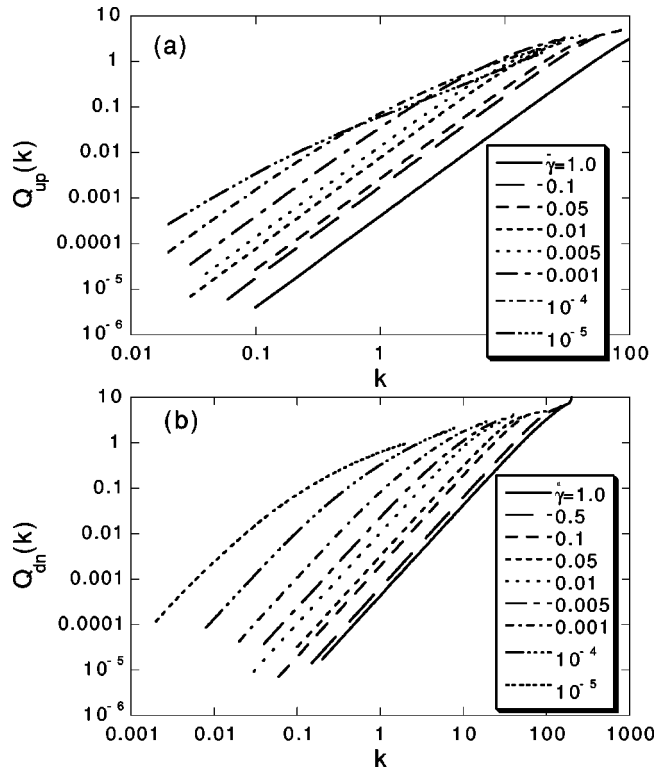


FIG. 15. Fourier transform of the velocity distribution, the function $Q(k)$ as defined by Eq. (8), for velocities collected while the total elastic energy is increasing, Q_{up} , and decreasing, Q_{dn} . As $\dot{\gamma}$ decreases, Q_{up} and Q_{dn} deviate from a power law of k^2 (Gaussian behavior) at smaller and smaller values of k .

($\dot{\gamma} < \dot{\gamma}_x$), rearrangement events involving several bubbles lead to a non-Gaussian tail. At very low shear rates, the distribution arises entirely from rearrangement events. The observation of a non-Gaussian velocity distribution is the reminiscent of recent results for driven granular gases [29–32], although it is not clear for all geometries that granular gases approach a Gaussian distribution at high driving rates.

The rest of this section is devoted to the nature of the distribution at low shear rates. It proves useful to Fourier transform the velocity distribution:

$$\bar{P}(k) \equiv \frac{1}{\pi} \int_0^{\infty} d\Delta v_y P(\Delta v_y) \cos(k\Delta v_y). \quad (7)$$

We define the function

$$Q(k) \equiv -\ln \bar{P}(k). \quad (8)$$

When $P(\Delta v_y)$ is Gaussian, then $Q(k)$ is a straight line with a slope of 2 on a log-log plot, with a prefactor of $\delta v^2/2$. The functions $Q_{up}(k)$ and $Q_{dn}(k)$ are derived from $P_{up}(\Delta v_y)$ and $P_{dn}(\Delta v_y)$ through Eqs. (7) and (8). Figure 15(a) shows $Q_{up}(k)$ vs k for several different shear rates. As expected, $Q_{up}(k)$ is a straight line with a slope of 2 at high shear rates. As $\dot{\gamma}$ decreases below ≈ 0.01 – 0.05 , however, we find that $Q_{up}(k)$ deviates away from a power law of 2 at high k . At low k , however, $Q_{up}(k)$ is still approximately $s_{up}^2 k^2/2$ for $\dot{\gamma}$

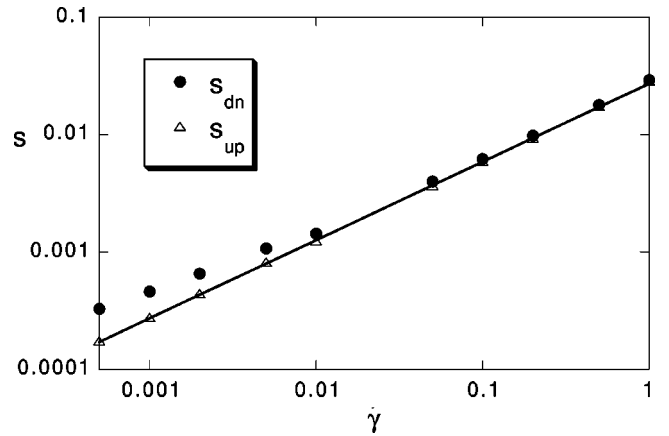


FIG. 16. Coefficient s of k^2 at low k for $Q_{up}(k)$ (triangles) and $Q_{dn}(k)$ (circles). The straight line is a fit to s_{up} to a power law of 0.67.

$\geq 5 \times 10^{-4}$, and we can extract the coefficient s_{up} . When a similar procedure is carried out for $Q_{dn}(k)$, it leads to similar results. The resulting values of s_{up} and s_{dn} are plotted in Fig. 16. For $\dot{\gamma} \geq 0.01$ – 0.05 , both distributions are Gaussian so Q_{up} and Q_{dn} are pure power laws with exponent $\alpha=2$ and $s_{up}=s_{dn}$. Below $\dot{\gamma} \approx 0.01$, however, Q_{up} and Q_{dn} both deviate from the Gaussian behavior at high k , and the coefficients s_{up} and s_{dn} obtained from fits to Q_{up} and Q_{dn} at low k are no longer identical to each other. Figure 16 shows that $s_{dn} > s_{up}$ at low shear rates. Note that we also find that s_{up} is a power law in $\dot{\gamma}$ over the entire range of shear rates, with an exponent of $\approx 2/3$, as shown by the dotted line. This is consistent with results on other driven athermal systems such as granular media, where the magnitude of velocity fluctuations (e.g., the granular temperature) scales sublinearly with the driving velocity [23–26].

At shear rates below 5×10^{-4} , the low- k behavior is no longer a power law with an exponent of $\alpha=2$, so we can no longer extract s_{up} or s_{dn} . It is possible that this is because the statistics are poor at high velocities. This speculation is supported by the observation that the power-law behavior at low k disappears at even higher shear rates for shorter runs or smaller systems. Although we cannot extract s_{up} , we can extrapolate the power-law behavior shown in Fig. 16 to shear rates below 5×10^{-4} . Then, if we define $\bar{Q}_{up}(k) \equiv Q_{up}(k)/s_{up}^2$ at all shear rates, we see that the low- k behavior is independent of the shear rate, as shown in Fig. 17. This plot suggests that as $\dot{\gamma}$ decreases below $\dot{\gamma} = 0.01$, the high- k behavior of $\bar{Q}_{up}(k)$ crosses over to a smaller power law. The plot also suggests that for k less than some value, say k_{low} , Q_{up} scales as k^2 (Gaussian behavior), but that the value of k_{low} decreases with decreasing shear rate.

Figure 18(a) shows $Q_{up}(k)$ together with speculative asymptotic fits to the high- k and the low- k behavior. The high- k asymptotic curve corresponds to a power law with $\alpha=1$ (Cauchy distribution) and the low- k asymptotic curve corresponds to a power law with $\alpha=2$ (Gaussian distribution), obtained by extrapolating the power-law fit to s_{up} shown in Fig. 16. The same Cauchy and Gaussian distribu-

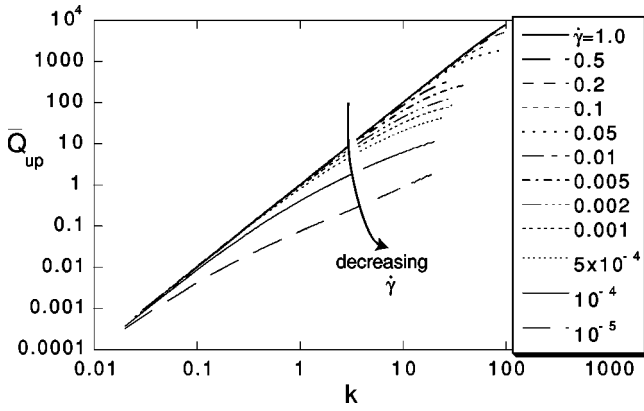


FIG. 17. Fourier transform of the velocity distribution, $Q_{up}(k)$, scaled to collapse at low k , where $Q_{up}(k)$ is proportional to k^2 (Gaussian behavior).

tions are shown in real (velocity) space in Fig. 18(b) together with the distribution $P_{up}(\Delta v_y)$. The distribution follows a Cauchy distribution fairly well at small velocities, but is cut off at high velocities. It is possible that the system crosses over to a pure Cauchy distribution in the limit $\dot{\gamma} \rightarrow 0$, and that the cutoff at low k gets squeezed down to $k=0$. Another possibility is that the Fourier transform of the distribution approaches a pure power law with a somewhat higher expo-

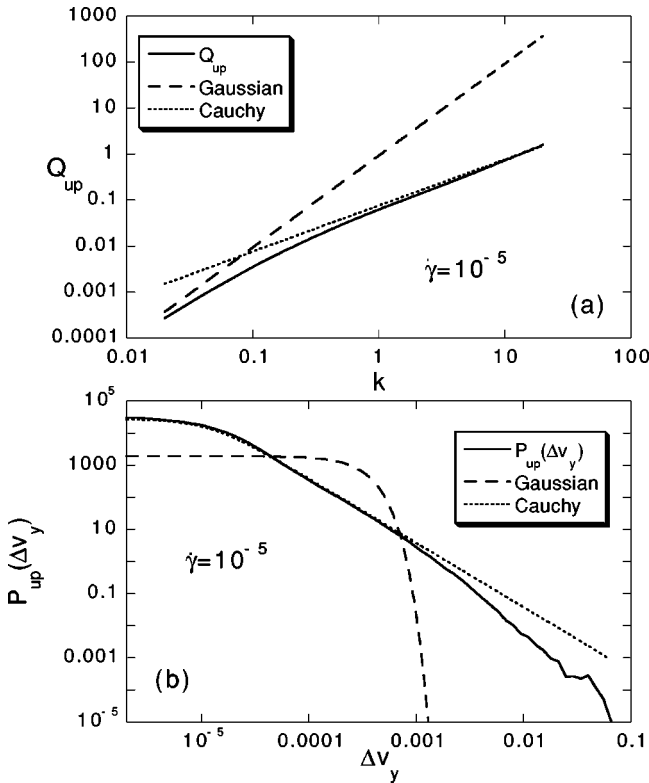


FIG. 18. (a) Fourier transform of velocity distribution, Q_{up} , at a shear rate of $\dot{\gamma} = 10^{-5}$, along with fits to the limiting low- k behavior (Gaussian), obtained by extrapolating the curve in Fig. 16, and to the high- k limiting behavior (Cauchy distribution). The corresponding velocity distribution is shown in (b), together with the same Gaussian and Cauchy fits in velocity space.

nent (we find that 1.1 provides a better fit). A distribution with $Q(k)$ given by a pure power law with an exponent $\alpha < 2$ is known as a Levy distribution (the Cauchy distribution is a special case of the Levy distribution, with $\alpha=1$) [41]. Despite our results, which are consistent with a Levy distribution, we suspect that this is not the final limiting behavior at vanishing shear rate. A Levy distribution has diverging moments. We speculate that there is an intrinsic cutoff to the divergence set by a typical maximum velocity of a bubble during a rearrangement event, which is roughly the correlation length for velocity fluctuations, $\bar{\xi}$, divided by the correlation time τ . Physically, this velocity scale is roughly a bubble diameter divided by the duration of a rearrangement event. In our units, the system size is $L=1$, the time scale set by the spring constant and the friction coefficient is $\tau=1$, and the characteristic velocity $\bar{\xi}/\tau$ is $v_{max} \approx 0.01$. This is the upper end of the velocity fluctuations that we can observe at low shear rates (see Fig. 11), given our computational resources.

In general, one would expect higher velocities during rearrangement events when the elastic energy is decreasing. Therefore, one would expect the distribution $P_{dn}(\Delta v_y)$ to be broader than $P_{up}(\Delta v_y)$. This is indeed the case at low shear rates, as shown by Fig. 19(a) for $\dot{\gamma} = 10^{-5}$. The arrows mark the values of s_{up} and s_{dn} obtained from the low- k behavior of Q_{up} and Q_{dn} . These parameters are also plotted in Fig. 16, which shows that s_{up} decreases relative to s_{dn} with decreasing shear rate. The statistics are not as good for s_{dn} as for s_{up} at low shear rates, but the discrepancy between s_{dn} and s_{up} cannot be accounted for by the difference in statistics. We believe that the difference reflects the true dynamics of the system: s_{dn} contains large velocities that occur during rearrangement events, while s_{up} does not. We have not characterized the distribution P_{dn} further; its Fourier transform Q_{dn} does not appear to obey a power law at high k , as shown in Fig. 15(b), although it may approach a power law of ≈ 0.5 at high k and low $\dot{\gamma}$.

Note that $s_{up} = s_{dn}$ for shear rates $\dot{\gamma} \geq 0.01$. We also find that $P_{up} = P_{dn}$ in this regime, as shown in Fig. 19(b). This is not surprising; at high shear rates, all the bubbles keep rearranging all the time, so there is no distinction between the bubble motion when the energy is decreasing and increasing. It is only at lower shear rates when the bubble motion is punctuated by well-separated, intermittent rearrangements that there is a significant difference between the two distributions.

We note that during a large rearrangement event, it is possible for the energy to increase slightly for a short time even though there is an overall drop in the energy over the period of the entire event. The motion during the energy increase would be captured in P_{up} . The original purpose of sorting the velocity fluctuations into two distributions, depending on whether the total energy was increasing or decreasing, was to isolate rearrangement events into P_{dn} . However, this picture is a simplistic one because the total energy might be increasing even during a rearrangement event. Thus, P_{up} must still contain some rearrangement events. Even though the original motivation for breaking the

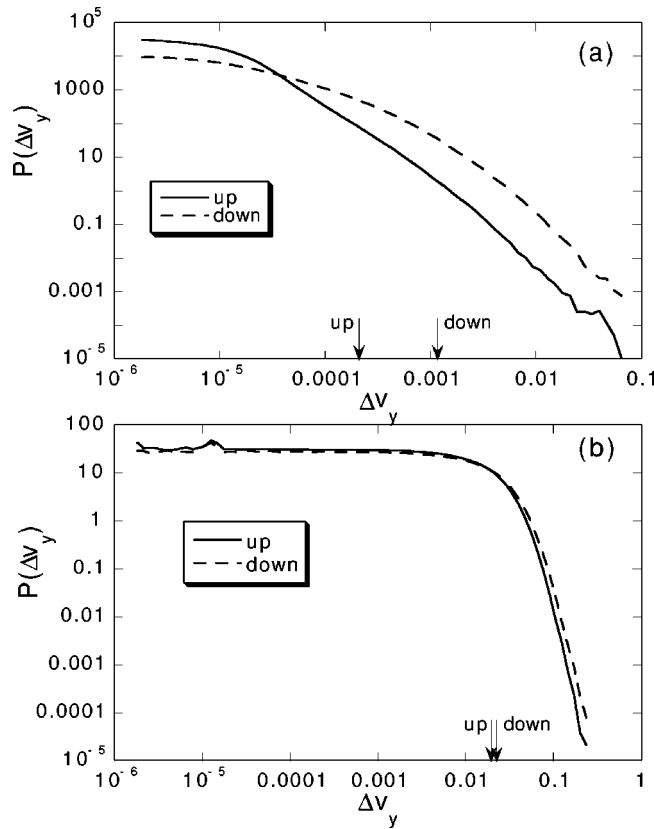


FIG. 19. The velocity distributions collected when the total energy is increasing (P_{up}) and decreasing (P_{dn}), respectively. The arrows mark the coefficients s_{up} and s_{dn} of k^2 obtained by fitting Q_{up} and Q_{dn} , respectively, at low k . These coefficients provide a measure of the width of the distributions. (a) The distributions at a low shear rate of $\dot{\gamma} = 10^{-5}$. (b) The distributions at a high shear rate of $\dot{\gamma} = 10^{-2}$.

distribution into two parts appears to be naive, there is another reason to study P_{up} . Recall from Fig. 1(b) that the average duration of energy drops decreases as a power law with shear rate relative to the average duration of energy rises. This implies that the energy is decreasing only during a vanishing fraction of the time as $\dot{\gamma} \rightarrow 0$. As a result, the full distribution approaches P_{up} in the limit of vanishing shear rate [$P(\Delta v_y) \rightarrow P_{up}(\Delta v_y)$ as $\dot{\gamma} \rightarrow 0$].

We have also collected the velocity fluctuation distribution in the x direction (the shear velocity direction), $P(\Delta v_x)$. The behavior of $P(\Delta v_x)$ is qualitatively the same as the behavior of $P(\Delta v_y)$ described above. At low shear rates $\dot{\gamma} \leq 0.01$, the two distributions $P(\Delta v_x)$ and $P(\Delta v_y)$ are identical. For $\dot{\gamma} \geq 0.01$, $P(\Delta v_x)$ is Gaussian, but with a standard deviation σ_x that is slightly greater than σ_y , as shown in Fig. 20. This could be due to the tendency of the bubbles to organize into strings at high shear rates, as evidenced by movies of the simulations. Once the particles organize into strings moving in the shear direction, one would expect fluctuations in the y direction to be suppressed relative to fluctuations in the x direction.

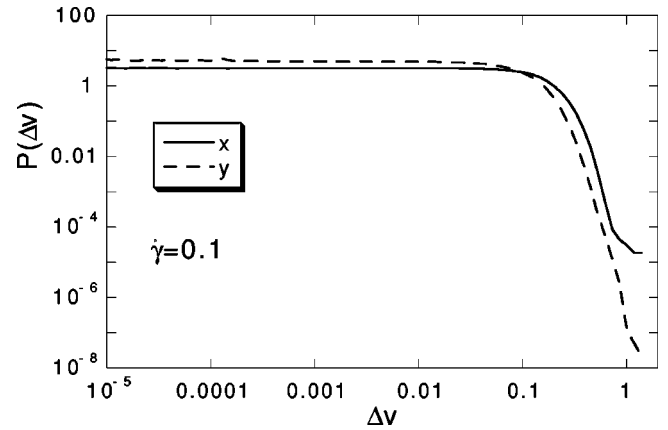


FIG. 20. Velocity distributions $P(\Delta v_x)$ and $P(\Delta v_y)$ of fluctuations in the x and y directions, respectively. At high shear rates, these are not quite the same; the distribution is broader in the x direction.

V. DISCUSSION

We have shown that the character of velocity fluctuations changes markedly at a crossover shear rate $\dot{\gamma}_x$. We have argued that these changes arise from the crossover from smooth flow to intermittent rearrangement events, and that rearrangement events completely control the behavior in the zero shear rate limit. Based on this argument, one would expect $\dot{\gamma}_x = \gamma_y / \tau_d$, where $\gamma_y \approx 0.01$ is the yield strain and $\tau_d = 1$ is the duration of a rearrangement event (in our units). Above γ_y / τ_d , the duration of a rearrangement event exceeds the time between rearrangements, so the flow should be smooth. Below γ_y / τ_d , the rearrangement events are separated in time. This prediction agrees well with our observations. Above $\dot{\gamma}_x$, the velocity fluctuations are exponentially correlated in space and time, and follow a Gaussian distribution. Below $\dot{\gamma}_x$, the velocity fluctuations decay more slowly than exponentially in space and time, and follow a distribution that is broader than Gaussian.

In addition to qualitative observations of the shapes of distributions and correlation functions, we have gathered considerable quantitative information on how various quantities depend on the shear rate. These quantities include τ_e and ξ_e , the time and length scales over which the velocity correlations decay to $1/e^2$ of their original value at $t=0$ and $r=0$ [Figs. 4(c) and 5(c)], as well as the diffusion coefficient D (Fig. 9) and the standard deviation of velocity fluctuations, δv (Fig. 2). In previous studies, we have obtained the shear stress σ_{xy} , the elastic energy E , and the standard deviation of elastic energy fluctuations, δE , as a function of shear rate. We first note that the behavior of ξ_e is trivial, in which ξ_e is always approximately the bubble diameter, and increases by only a factor of 2 or so over the entire range (four decades) of shear rate. We will therefore consider the bubble diameter d to be the only important length scale. We will now show that the measured quantities are tied together over the entire range of shear rates through a few simple relationships that yield insight into the nature of foam dynamics under shear.

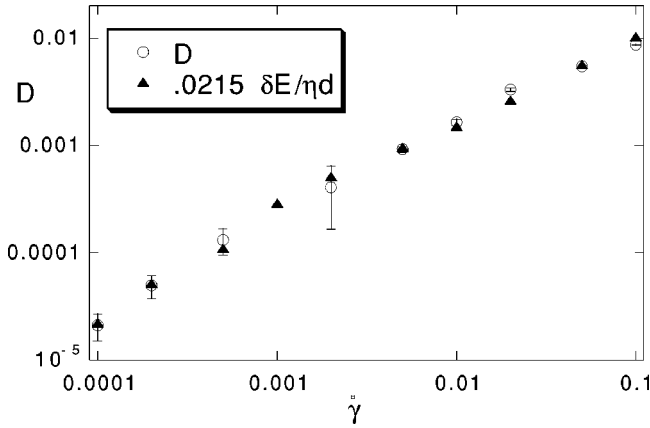


FIG. 21. The Stokes-Einstein relation. The open circles represent the diffusion coefficient calculated from the y displacement distribution. The triangles represent the standard deviation of the elastic energy, δE , divided by the viscosity and average bubble diameter, up to a constant coefficient of 0.0215. The excellent agreement between the circles and triangles shows that the Stokes-Einstein relation is obeyed with an effective temperature proportional to δE .

A. Stokes-Einstein relation

The behavior of the self-diffusion coefficient of a bubble in the transverse direction D_y is shown as a function of shear rate in Fig. 9. Note that D_y increases with $\dot{\gamma}$. This is in accord with our expectations: the diffusion coefficient arises from the jostling of bubbles under shear flow, so it should increase with $\dot{\gamma}$ and vanish in the limit $\dot{\gamma} \rightarrow 0$. Figure 9 shows that the behavior of D_y is not a simple power law in $\dot{\gamma}$. To gain insight into the dependence of D_y on shear rate, we have measured the viscosity of the shear-thinning foam, $\eta(\dot{\gamma})$, and the fluctuations in the elastic energy of the bubbles, $\delta E^2 \equiv \langle (\Delta E)^2 \rangle$. The latter quantity increases with shear rate because there are more overlaps between bubbles. We find that

$$D = C \frac{\delta E}{\eta d}, \quad (9)$$

where d is the average bubble radius and $C = 0.0215$. Both sides of the above equation are plotted as a function of shear rate in Fig. 21. The expression in Eq. (9) has the same form as the Stokes-Einstein equation for thermal particles, with δE instead of the thermal energy kT . This suggests that fluctuations in the elastic energy give the bubbles random kicks that cause them to diffuse. In other words, diffusion in our driven athermal system resembles diffusion in a thermal system with an effective temperature given by the scale of potential energy fluctuations. In another paper, we have measured effective temperatures based on various linear-response relations, and have shown that $D = C' T_{\text{eff}} / \eta d$ [12]. Thus, the scale of energy fluctuations sets the scale of the effective temperature.

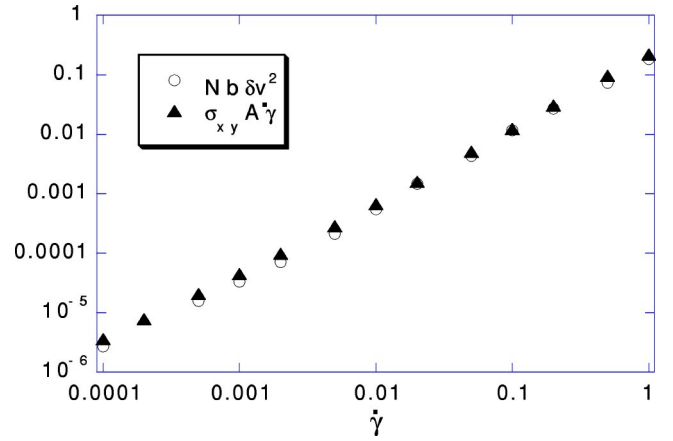


FIG. 22. The magnitude of velocity fluctuations is set by the power supplied to the system. The power supplied by the shear (triangles) is dissipated by velocity fluctuations (circles).

B. Power balance

In a steady-state sheared system, all the power supplied to the system must be dissipated. This provides a scaling relation between the shear stress and the velocity fluctuations. The power supplied by the external driving force is given by $\sigma_{xy} \dot{\gamma} A$, where $\sigma_{xy} \dot{\gamma}$ is the power supplied per unit area and A is the area of the system. The power dissipated by the flow arises from the velocity difference between the bubble velocity and the average velocity due to the shear flow at the position of the bubble. The typical force between neighboring bubbles is $b \delta v$, where $b \equiv 1$ is the friction coefficient in the model and δv is the characteristic velocity fluctuation (the standard deviation of velocity fluctuation distribution). The power dissipated is the dot product of the force and the velocity, so it is $b \delta v^2$ for each bubble, or $N b \delta v^2$ altogether. Thus, we have the relation

$$\sigma_{xy} \dot{\gamma} A = N b \delta v^2. \quad (10)$$

We have verified that this relation does indeed hold for our system by plotting the left and right hand sides of Eq. (10) as a function of shear rate in Fig. 22. The agreement is excellent.

C. Final remarks

This study highlights the importance of the crossover shear rate $\dot{\gamma}_x = \gamma_y / \tau_d$, the yield strain divided by the duration of a rearrangement event. A number of quantities have been shown previously to exhibit a crossover at $\dot{\gamma}_x$ within the model. We have compiled all the quantities into Table I. In each case, deviations from the high shear rate behavior appear at shear rates of 0.01 or 0.02, and the limiting low shear rate behavior is reached around $\dot{\gamma} = 10^{-3}$. It is important to recognize that although there appears to be a change of behavior at $\dot{\gamma}_x$, the crossover shear rate is not necessarily well defined. The value of the yield strain γ_y depends on the time scale on which the stress is measured. Thus, there is some ambiguity in $\dot{\gamma}_x$, similar to the ambiguity that arises in studies of the glass transition.

TABLE I. Quantities that exhibit a change of behavior around $\dot{\gamma}_x$ according to simulations on the Durian model. The numbers following each quantity indicate the reference in which the behavior was discussed.

Quantity	Behavior above $\dot{\gamma}_x$	Behavior below $\dot{\gamma}_x$
Energy [8,9]	Increases with $\dot{\gamma}$	Approximately independent of $\dot{\gamma}$
Shear stress [8,9]	Increases with $\dot{\gamma}$	Approximately independent of $\dot{\gamma}$
T_{eff} [11,12]	Increases with $\dot{\gamma}$	Approximately independent of $\dot{\gamma}$
Avalanche distributions [10]	Depend on $\dot{\gamma}$	Approximately independent of $\dot{\gamma}$
Rearrangement event rates [10]	Depend on $\dot{\gamma}$	Approximately independent of $\dot{\gamma}$
Viscosity [11]	Arrhenius in T_{eff}	Super-Arrhenius in T_{eff}
Velocity distribution	Gaussian	Broader than Gaussian
$C(t)$ [see Eq. (1)]	Exponential decay	Slower-than-exponential decay
$F(r)$ [see Eq. (1)]	Exponential decay	Slower-than-exponential decay

Experiments on both foams [21,33] and emulsions [6] show a crossover in the behavior of the shear stress, similar to that seen in simulations [8,9], where the shear stress decreases with decreasing $\dot{\gamma}$ down to $\dot{\gamma}_x$ and then levels off. Measurements on a commercial shaving cream [5,16,21] and on bubble rafts [33] show that the stress exhibits a crossover in shear rate dependence from one power law to another near a characteristic shear rate of $\dot{\gamma}_x = 0.1 \text{ s}^{-1}$. Below this shear rate, rearrangement events in a three-dimensional foam can be resolved using diffusing-wave spectroscopy; above $\dot{\gamma}_x$, the flow appears to be affine [5,16]. The response to a step strain imposed on top of the steady shear also changes with shear rate [21]: the instantaneous shear modulus is zero above $\dot{\gamma}_x$ and nonzero below. Finally, there is a qualitative change in the nature of fingering patterns observed when gas is pumped into a foam [34]. For shear rates above $\dot{\gamma}_x$, the fingering pattern is smooth and viscous in character, while for shear rates below $\dot{\gamma}_x$, it is jagged and elastic.

In simulations of model glassforming liquids such as Lennard-Jones mixtures, a similar crossover is observed as a function of *temperature*: dynamical correlation functions are exponential above a characteristic temperature T_x and stretched exponential below T_x , the viscosity is Arrhenius above T_x and super-Arrhenius below T_x [37,38], the potential energy of inherent structures is constant above T_x and decreases with T below T_x [35,36], kinetic heterogeneities appear below T_x [38,39], and translational diffusion, relaxation, and rotational diffusion become decoupled below T_x [38,39].

The resemblance of behavior near the crossover strain rate $\dot{\gamma}_x$ to behavior near the crossover temperature in supercooled liquids, T_x , raises the question of whether sheared systems can be described as thermal ones. A number of driven particulate systems, such as shaken granular materials [32,40], sedimenting colloids [42], and gas-fluidized particles [43] show surprisingly a thermal behavior. In some ways, velocity fluctuations in the system studied here are profoundly different from velocity fluctuations in an equilibrium, thermal, Hamiltonian system. In our system, there are nontrivial spatial correlations of the velocity; in an equilibrium system, these would vanish due to separation of position and momen-

tum terms in the Hamiltonian. In our system, the velocity distribution is definitely not Gaussian at shear rates below $\dot{\gamma}_x$; in a thermal system, the distribution is always Gaussian because the Hamiltonian is always quadratic in momentum. Nonetheless, there are some important and striking ways in which the behavior of our system is similar to that of a thermal system. The self-diffusion coefficient in the direction transverse to shear D_y satisfies a Stokes-Einstein relation with the thermal energy kT replaced by the characteristic potential energy fluctuation δE . Moreover, we have found that the idea of an effective temperature is useful; definitions of temperature calculated from different linear-response relations yield the same result [12].

When might the idea of an effective temperature be useful? We have proposed a criterion [12] based on the fluctuation-dissipation relation. In an equilibrium system, the amount of dissipation in the system is controlled by the amplitude of fluctuations. In a driven dissipative system, we can turn this around and ask whether the amount of dissipation controls the amplitude of fluctuations. We can answer this by studying the power dissipated by the system. In steady state, the power supplied to the system must be balanced, on an average, by the power dissipated. The power can be dissipated in two ways—by the average flow and by fluctuations around the average flow. If nearly all the power supplied by the driving force is dissipated by fluctuations, then the amplitude of fluctuations is controlled by the amount of dissipation, and there is a fluctuation-dissipation relation. On the other hand, if not all the power is dissipated by fluctuations, then the fluctuations are smaller than that allowed by the amount of dissipation and the relation breaks down. Thus, we speculated [12] that the concept of effective temperature is useful only if nearly all the power supplied by the driving force is dissipated by fluctuations. In this paper, we have shown that the width of the velocity distribution, δv , increases less rapidly than the shear rate (see Fig. 2). In particular, we find $\delta v \sim (\dot{\gamma}d)^\beta$, where $\beta \approx 0.6$. A similar sublinear scaling occurs in systems other than foams. In granular materials, a similar sublinear scaling of the velocity fluctuations (the granular temperature) with respect to the average flow was observed in hopper flows [23], surface flows [24], and shear flows [30,26] with similar

exponents (ranging from 0.5 to 0.7).

The sublinear scaling is important because it suggests that at high flow rates, fluctuations become negligible relative to the average flow and the idea of an effective temperature should fail. This may seem surprising, given our results for the velocity distributions, which become Gaussian at high shear rates and therefore appear more “thermal.” It is important to recall, however, that the particles in our simulations are massless, so the implications of the velocity distribution for an effective temperature are not clear.

Conversely, the sublinear scaling of velocity fluctuations with average velocity implies that in the limit of zero flow, the fluctuations diverge relative to the average flow. This implies stick-slip behavior, which is a hallmark of nearly

jammed systems. Thus, our arguments suggest that the concept of effective temperature should be most useful for systems near the onset of jamming.

ACKNOWLEDGMENTS

We thank Douglas Durian and Corey S. O’Hern for valuable comments and assistance on this project. We also thank Daniel Kivelson and Sidney Nagel for instructive discussions. This work was supported by the National Science Foundation through Grant. Nos. PHY-9407194 (S.A.L., A.J.L.), and CHE-9624090 and DMR-0087349 (S.T., I.K.O., A.J.L.).

-
- [1] *Foams: Theory, Measurement, and Application*, edited by R.K. Prud’homme and S.A. Khan, Surfactant Science Series Vol. 57 (Marcel Dekker, New York, 1996).
- [2] D.J. Durian and D.A. Weitz, in *Kirk-Othmer Encyclopedia of Chemical Technology*, 4th ed., edited by J.I. Kroschwitz (Wiley, New York, 1994), Vol. 11, pp. 783–805.
- [3] D. Weaire and N. Rivier, *Contemp. Phys.* **25**, 55 (1984).
- [4] A.M. Kraynik, *Annu. Rev. Fluid Mech.* **20**, 325 (1988).
- [5] A.D. Gopal and D.J. Durian, *Phys. Rev. Lett.* **75**, 2610 (1995).
- [6] T.G. Mason, J. Bibette, and D.A. Weitz, *J. Colloid Interface Sci.* **179**, 439 (1996).
- [7] P. Hébraud, F. Lequeux, J.P. Munch, and D.J. Pine, *Phys. Rev. Lett.* **78**, 4657 (1997).
- [8] D.J. Durian, *Phys. Rev. Lett.* **75**, 4780 (1995).
- [9] D.J. Durian, *Phys. Rev. E* **55**, 1739 (1997).
- [10] S. Tewari, D. Schiemann, D.J. Durian, C.M. Knobler, S.A. Langer, and A.J. Liu, *Phys. Rev. E* **60**, 4385 (1999).
- [11] S.A. Langer and A.J. Liu, *Europhys. Lett.* **49**, 68 (2000).
- [12] I.K. Ono, C.S. O’Hern, D. J Durian, S.A. Langer, A.J. Liu, and S.R. Nagel, *Phys. Rev. Lett.* **89**, 095703 (2002).
- [13] F. Bolton and D. Weaire, *Phys. Rev. Lett.* **65**, 3449 (1990).
- [14] C.S. O’Hern, S.A. Langer, A.J. Liu, and S.R. Nagel, *Phys. Rev. Lett.* **88**, 075507 (2002).
- [15] *Jamming and Rheology*, edited by A.J. Liu and S.R. Nagel (Taylor&Francis, New York, 2001), and references therein.
- [16] A.D. Gopal and D.J. Durian, *J. Colloid Interface Sci.* **213**, 169 (1999).
- [17] M. Dennin and C.M. Knobler, *Phys. Rev. Lett.* **78**, 2485 (1997).
- [18] J. Lauridsen, M. Twardos, and M. Dennin, *Phys. Rev. Lett.* **89**, 098303 (2002).
- [19] D. Lacks, *Phys. Rev. Lett.* **87**, 225502 (2001).
- [20] DDRIV3 is available from <http://gams.nist.gov> and SPARKIT2 was obtained from <ftp://ftp.cs.umn.edu>
- [21] A.D. Gopal and D.J. Durian, e-print cond-mat/0208181.
- [22] G. Debrégeas, H. Tabuteau, and J.-M. di Meglio, *Phys. Rev. Lett.* **87**, 178305 (2001).
- [23] N. Menon and D.J. Durian, *Science* **275**, 1920 (1997).
- [24] P.A. Lemieux and D.J. Durian, *Phys. Rev. Lett.* **85**, 4273 (2000).
- [25] W. Losert, L. Bocquet, T.C. Lubensky, and J.P. Gollub, *Phys. Rev. Lett.* **85**, 1428 (2000).
- [26] D. Mueth, *Phys. Rev. E* **67**, 011304 (2003).
- [27] J.E. Variyar, D. Kivelson, G. Tarjus, and J. Talbot, *J. Chem. Phys.* **96**, 593 (1992); J.E. Variyar, D. Kivelson, and R.M. Lynden-Bell, *ibid.* **97**, 8549 (1992).
- [28] S. Butler and P. Harrowell, *Phys. Rev. E* **54**, 457 (1996).
- [29] J.S. Olafsen and J.S. Urbach, *Phys. Rev. E* **60**, R2468 (1999).
- [30] W. Losert *et al.*, *Chaos* **9**, 682 (1999).
- [31] A. Kudrolli and J. Henry, *Phys. Rev. E* **62**, R1489 (2000).
- [32] F. Rouyer and N. Menon, *Phys. Rev. Lett.* **85**, 3676 (2000).
- [33] E. Pratt and M. Dennin, *Phys. Rev. E* **67**, 051402 (2003).
- [34] S.S. Park and D.J. Durian, *Phys. Rev. Lett.* **72**, 3347 (1994).
- [35] S. Sastry, *PhysChemComm* **1-14**, 79 (2000).
- [36] S. Sastry, P.G. Debenedetti, and F.H. Stillinger, *Nature (London)* **393**, 554 (1998).
- [37] W. Kob and H.C. Andersen, *Phys. Rev. E* **51**, 4626 (1995); **52**, 4134 (1995).
- [38] D.N. Perera and P. Harrowell, *Phys. Rev. Lett.* **81**, 120 (1998); *Phys. Rev. E* **59**, 5721 (1999).
- [39] S.C. Glotzer, V.N. Novikov, and T.B. Schröder, *J. Chem. Phys.* **112**, 509 (2000).
- [40] G. D’Anna and G. Gremaud, *Nature (London)* **413**, 407 (2001).
- [41] *Levy Flights and Related Topics in Physics*, edited by M.F. Shlesinger, G.M. Zaslavsky, and U. Frisch (Springer-Verlag, Berlin, 1995).
- [42] P.N. Segré, F. Liu, P. Umbanhowar, and D.A. Weitz, *Nature (London)* **409**, 594 (2001).
- [43] R.P. Ojha and D.J. Durian (unpublished).